coatings

MDPI

Article

Novel Anodic TiO_2 Synthesis Method with Embedded Graphene Quantum Dots for Improved Photocatalytic Activity

Ainars Knoks *, Liga Grinberga and Janis Kleperis

Institute of Solid State Physics, University of Latvia, LV-1063 Riga, Latvia; janis.kleperis@cfi.lu.lv (J.K.)
* Correspondence: ainars.knoks@cfi.lu.lv

Abstract: Photocatalytic degradation of pollutants have a high potential for sustainable and renewable uses. TiO_2 is a widely studied photocatalyst due to its high chemical and photochemical stability and wide range of applications. However, the wide band gap and low capacity of photo-induced charge separation provide lower catalytic activity; thus, improvement of these properties must be found. The doping of TiO_2 with other elements, such as carbon nanoparticles (CNP) in a quantum dot form, offers a promising pathway to improve the aforementioned properties. In addition, in situ doping methods should be investigated for practical scalability, as they offer the advantage of integrating dopants directly during material synthesis, ensuring a more uniform distribution and better interaction between the dopant and the host material, in turn leading to more consistent photocatalytic properties. Current technologies primarily involve nanoparticle combinations. This work focuses on the development of a novel in situ synthesis methodology by the introduction of three different graphene-based quantum nanodots into anodic TiO_2 and the following investigation of structural, morphological, and photocatalytic properties. Results indicate that the introduction of CNP allows for the shift of a set of parameters, such as the optical band gap, increased photo-induced charge carrier density of TiO_2/CNP composite, and, most importantly, the change of crystalline phase composition depending on added CNP material. Research indicates that not only a higher concentration of added CNP enhances higher photocatalytic activity as tested by the degradation of methylene blue dye, but also the type of CNP determines final crystalline phase. For the first time brookite and rutile phases were obtained in anodic titania synthesized in inorganic electrolyte by introducing hydrothermally treated exfoliated graphene.

Keywords: anodic TiO_2; carbon nanoparticles; doped TiO_2; photocatalysis; composite

Citation: Knoks, A.; Grinberga, L.; Kleperis, J. Novel Anodic TiO_2 Synthesis Method with Embedded Graphene Quantum Dots for Improved Photocatalytic Activity. *Coatings* **2024**, *14*, 1407. https://doi.org/10.3390/coatings14111407

Academic Editors: Chengkai Yang and Qian Wang

Received: 29 September 2024
Revised: 24 October 2024
Accepted: 2 November 2024
Published: 5 November 2024

1. Introduction

It is not a secret that the majority of our energy needs are met by fossil fuels [1], which are a major source of anthropogenic CO_2 released into the atmosphere. The rapidly increasing concentration of CO_2 is believed to be one of the causes of climate change [2], as evidenced by the rise in sea level [3] and by changes in natural habitats and the environment. These changes include decreasing oxygen content in the global ocean, leading to change in pH and in CO_2 absorption capability, which, in worst-case scenarios, can lead to anoxia [4]. Additionally, there are other aspects that need attention, such as the overall impact on treatability, e.g., pollution's influence on antibiotic resistance [5], and, more directly, on organic waste, including drug and medical byproducts and pesticides [6].

One foreseen way to mitigate the aforementioned problems is to decrease the energy demand in various aspects of life. Water treatment is energy demanding [7], especially in areas with fossil-fuel-based electricity production such as China, whether it be via direct [8] or hidden [9] emissions. The use of robust materials [10,11], particularly the reduction of various pollutants via the use of abundant energy sources, e.g., the photocatalytic degradation of pollutants using sunlight, would shift energy demand from an active demand to a more passive demand, thus, saving a substantial amount of energy/emissions. TiO_2

is a suitable material due to its wide availability, low toxicity, high chemical stability [12], and its large area of application, i.e., in CO_2 reduction [13], batteries [14,15], microbial fuel cells [16,17] and others. However, TiO_2 is known to have relatively low efficiency as a photocatalyst due to its wide band gap [18,19]. Specifically, titania has two major obstacles for wide photocatalytic use: a wide band gap, which requires irradiation with high energy photons (in the UV region), and a fast recombination of photo-induced charge carriers [20–22], which reduces photoactivity.

To improve the photocatalytic activity of TiO_2, its properties and parameters should be changed. Firstly, the optical absorption edge should be shifted to longer wavelengths, i.e., those in the visible range. Secondly, improving the separation of photo-induced charge carriers is crucial for increasing their lifetime. The enhancement can be achieved by introducing dopant materials into TiO_2 [23–25]. In addition, the dopant material should be accessible and abundant. Carbon nanomaterials, such as graphene and carbon nanoparticles (CNPs), have attracted attention. However, the production of graphene at scale faces technological obstacles, and is thus still under development. Some studies have reported methods for the electrochemical production of graphene and graphene quantum dots (GQDs) [26]. We can utilize the unique properties of GQDs to enhance the photocatalytic activity of the catalyst surface i.e., by increasing visible light response and utilizing hot electrons [27,28]. GQDs have applications in photocatalysis [29], optoelectronics [30,31], sensors [32], medicine, bio-imagining [33], and others. GQDs were initially discussed in the context of carbon materials and carbon nanodots, as described in [34]. Graphene is a zero bandgap semiconductor, and its band gap can be determined/tuned by the substrate [35,36]. GQDs graphene sheets composed of several layers and are a few nanometers wide. In addition, they have edge site effects, as well as quantum confinement, which may improve the photocatalytic properties of TiO_2. Similarly to graphene, GQD production/synthesis is not trivial. Current synthesis methods include hydrothermal and solvothermal techniques [32], electrochemical exfoliation, and thin layer techniques. Each method provides various challenges. For example, after exfoliation, graphene must be separated, and, to achieve true GQDs, these graphene sheet stacks require further separation and dispersion. Zhao et al. have demonstrated a three-step hydrothermal synthesis requiring high concentrations of HNO_3 [37]. Other methods include the oxidation of GO with a variety of agents, such as O_3 [38], hydrothermal cutting, [26,39], the photo-Fenton method [40] and ultrasonication [41]. As summarized by Pirsaheb et al. [42], the introduction of GQD enhances the photocatalytic properties of TiO_2.

The successful implementation of GQDs into anodic TiO_2 has yet to demonstrate its full utility. A successful integration of GQDs in titania nanoparticles has been demonstrated previously [43–45]. NP synthesis and use has advantages but it also has drawbacks, such as possible leeching into the environment, and technological complications in terms of filtration and recovery. These problems can be solved with nanostructured coatings, though the wide implementation of CNPs for coatings has not yet been demonstrated. A simplified synthesis process of catalyst with modifications is essential for large-scale application. Incorporating GQDs during the synthesis would streamline production and enhance scalability. In this work, a novel anodic TiO_2 composite synthesis method is developed to incorporate carbon nanoparticles into titania, thereby improving its photocatalytic activity. Titania has been synthesized and CNPs have been incorporated using a unique combination of anodization process and electrophoretic deposition. Morphology, structure, and photoelectrochemical properties were then investigated to compare synthesized and commercial GQD influence on TiO_2 properties.

2. Materials and Methods

All chemicals used in this research, including Ti foil, were purchased from Sigma-Aldrich. In this work, three carbon material additives were used in a developed in situ methodology that combines anodization and electrophoretic methods. The first additive was reduced graphene sheet stacks (for simplicity, referred to here as G), synthesized

by exfoliating metallurgically used graphite crucibles, followed by reduction in an inert atmosphere. The electrochemical exfoliation was performed in a H_2SO_4 solution, with a frequency-modulated voltage alternating every 10 s between two graphite electrodes to increase the yield, assuming SO_4^{2-} ions are responsible for the exfoliation process. After collecting a substantial amount of material, it was washed with deionized water, vigorously ultrasonicated (UP200St—Ultrasonic Lab Homogenizer, Hielscher Ultrasonics, Teltow, Germany) to break apart agglomerates, and dried in an ambient atmosphere at 60 °C. However, graphite used in metallurgy, as well as sulfur-based exfoliation electrolyte, introduced impurities into exfoliated material. Therefore, it was annealed in an Ar/H_2 atmosphere (Linde Gas SIA, Riga, Latvia) for 4 h at 900 °C (Snol tube furnace, SnolTherm, UAB, Narkunai, Lithuania). After annealing, the obtained G particles were dispersed in a nonpolar solvent (DMF) and ultrasonicated to break down particle size further until a homogeneous dispersion was achieved. An extensive description of the method, though with different electrolytes, is discussed in the work of Olins et al. [46]. To further reduce the particle size, the G material emulsion was placed in a stainless-steel autoclave with a Teflon chamber and heated at 140 °C for 8 h, followed by 200 °C for an additional 8 h for hydrothermal synthesis. The obtained material was designated as H. As a result, an emulsion with carbon nanoparticles, with an approximate size under 10 nm, was achieved. For comparison, commercial graphene quantum dots (Q) were purchased (Sigma-Aldrich, Saint Louis, MO, USA, green luminescence GQD in water 1mg/mL). These three carbon nanomaterials—G, H, and Q—were further used as additives in TiO_2 synthesis, with the samples then denoted as G, H, and Q appropriately.

TiO_2 was synthesized through the electrochemical anodization of Ti foil in F^- ion-containing water/H_3PO_4-based electrolyte, as described in [40]. The synthesis was modified to include two steps—anodizing at 25 V for 25 min and then again for 90 min. In the second step, CNP additives were introduced into the anodization electrolyte at various concentrations by adding 0.5, 1, 2, and 4 mL (concentration 1mg/mL) to 60 mL electrolyte. Before the introduction of additive CNP, the solutions were sonicated for even dispersion. After the addition, electrolyte was mixed throughout the synthesis process, which helped to prevent sedimentation and agglomeration. The method of composite synthesis in the organic electrolyte is detailed in our previous work, where commercial Pt-doped carbon and exfoliated N-doped graphene particles were used as additives, though no additional description of the synthesis process was elaborated [47].

Three sets of samples were synthesized and treated using identical parameters, differing only in the addition of carbon material at various amounts. The samples were designated as follows: G-material-added samples were identified as G 0, 1, 2, 3, 4; hydrothermal-synthesis-material-added samples were identified as H 0, 1, 2, 3, 4; and commercial graphene-quantum-dot-added samples were identified as Q 0, 1, 2, 3, 4. After synthesis, all samples were annealed in an Ar/H_2 atmosphere in the tube furnace at 500 °C for 120 min to achieve crystallization of TiO_2.

Photoelectrochemical properties were measured using on–off modulation cycles of light irradiation to measure both the open-circuit potential (OCP) and the photocurrent response (PCR). After reaching a steady state, the flat band potential (E_{Fb}) was determined in darkness by the Mott–Schottky method (MS) [48–51]. For light modulation, a 150W Xenon lamp (with UV cut off) was used, a VoltaLab potentiostat (Radiolab Analytica PGZ 301, Lyon, France) was exploited for the photoelectrochemical (PEC) measurements in 1 M NaOH, and a saturated calomel electrode (SCE) was used as a reference electrode. Morphology was investigated using scanning electron microscopy (Phenom Pro SEM, Phenom-World, Eindhoven, The Netherlands) and atomic force microscopy (AFM NT-MDT, model Smena, Moscow, Russia). The structural analysis was performed using X-ray diffraction (XRD RIGAKU MiniFlex 600 X-ray diffractometer, Tokyo, Japan) and Raman spectroscopy (TriVista CRS confocal Raman microscope, Spectroscopy & imaging GmbH, Bördestr, Germany). To estimate the band gap value of the samples, recorded reflectance spectra (Shimadzu SpecCord 9000 with integrating sphere, Kyoto, Japan) and Kubelka–

Munk transformation [52,53] was used. TiO_2 has an indirect allowed band gap; therefore, the transformation coefficient n = ½ was used.

The photocatalytic properties of synthesized samples were investigated through the degradation of methylene blue (MB). The 0.03 mM MB solution was prepared by dissolving MB in deionized water. Then, the sample was immersed in the MB and left to reach a steady state. Samples were irradiated using the same light source as in PEC measurements. The investigation of solution absorbance was achieved with chosen time intervals measured using the absorbance kit and software (OceanOptics HR4000, Ostfildern, Germany). Absorbance was measured before irradiation started and after reaching a steady state (chosen time for sample relaxation in MB solution allowing MB adsorption). The degradation coefficient (k) was then calculated from the linear slope coefficient of the plot

$$ln\frac{A_t}{A_0} = -kt$$

3. Results

The synthesized and purchased CNPs were investigated with AFM. In order to ensure comparable particle size evaluation, solutions had to be diluted. All samples for AFM were prepared in the same manner by dispersing small quantities, around 0.001 mL of material (H, G, and Q) solution in 20 mL of deionized water, then sonicated for 5 min for higher dispersion and to ensure a very low concentration. Then, using a precision paint spray gun for even distribution, the solution was sprayed on a silica wafer and allowed to dry. The AFM investigation results are depicted in Figure 1.

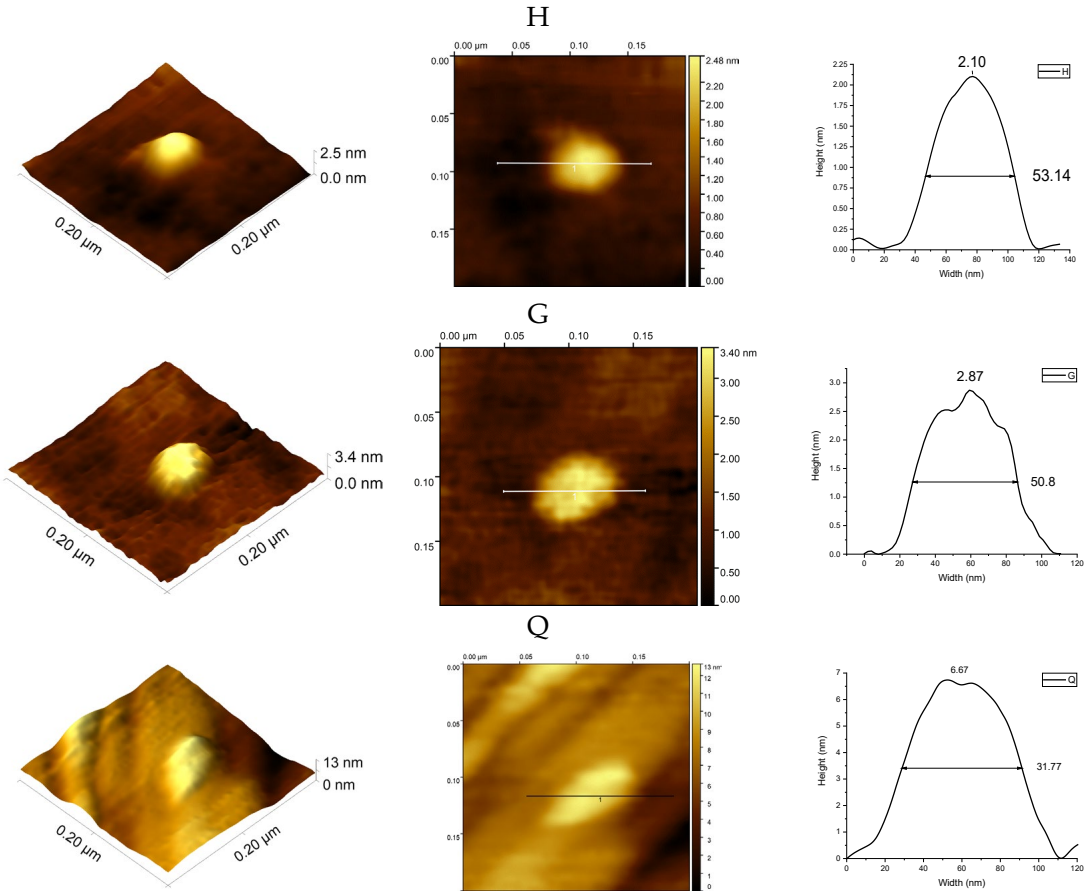

Figure 1. AFM investigation of synthesized (H, G) and purchased (Q) carbon nanomaterials.

As is seen from Figure 1, H particles measured approximately 2.0 nm in height and 53 nm in width, G measured 2.9 nm in height and 51 nm in width, and Q particles were

measured to be 6.6 nm in height and 32 nm in width. The large width suggests particle agglomeration after the deposition for testing during the drying process.

To incorporate CNP into titania during anodization, the z potential of the particles should be negative. The zeta potential measurements for used CNPs are shown in Table 1, with measurements carried out with the Litesizer^{TM} 500 (Anton Paar, Graz, Austria). Both the commercial and synthesized NPs have similar potentials, whereas G shows a more positive potential, indicating that G has a lower incorporation efficiency and possibly a higher agglomeration rate compared with other CNPs.

Table 1. Measured z potential and electrophoretic mobility.

CNP	Zeta Potential, mV	Negative Electrophoretic Mobility, μm·cm·Vs^{-1}
Q	−35.7 ± 5.4	1.79 ± 0.01
G	−5.0 ± 0.6	0.25 ± 0.01
H	−46.8 ± 2.3	2.35 ± 0.01

A structural investigation of synthesized composite samples was conducted using XRD and Raman spectroscopy (Figure 2). Table 2 shows the vibrational modes of synthesized samples, their comparison with the known TiO_2 anatase, and the rutile vibrational mode values. It is noteworthy that, for the H series, there are shifts of vibrational modes and additional shoulders, indicating possible phase mixtures, such as brookite or rutile, in addition to anatase. In the presence of brookite, the modes would be at A_{1g} (127, 154, 194, 247, 412, 640 cm^{-1}), B_{1g} (133, 159, 215, 320, 415, 502 cm^{-1}), B_{2g} (366, 395, 463, 584 cm^{-1}) and B_{3g} (452 cm^{-1}) [54,55].

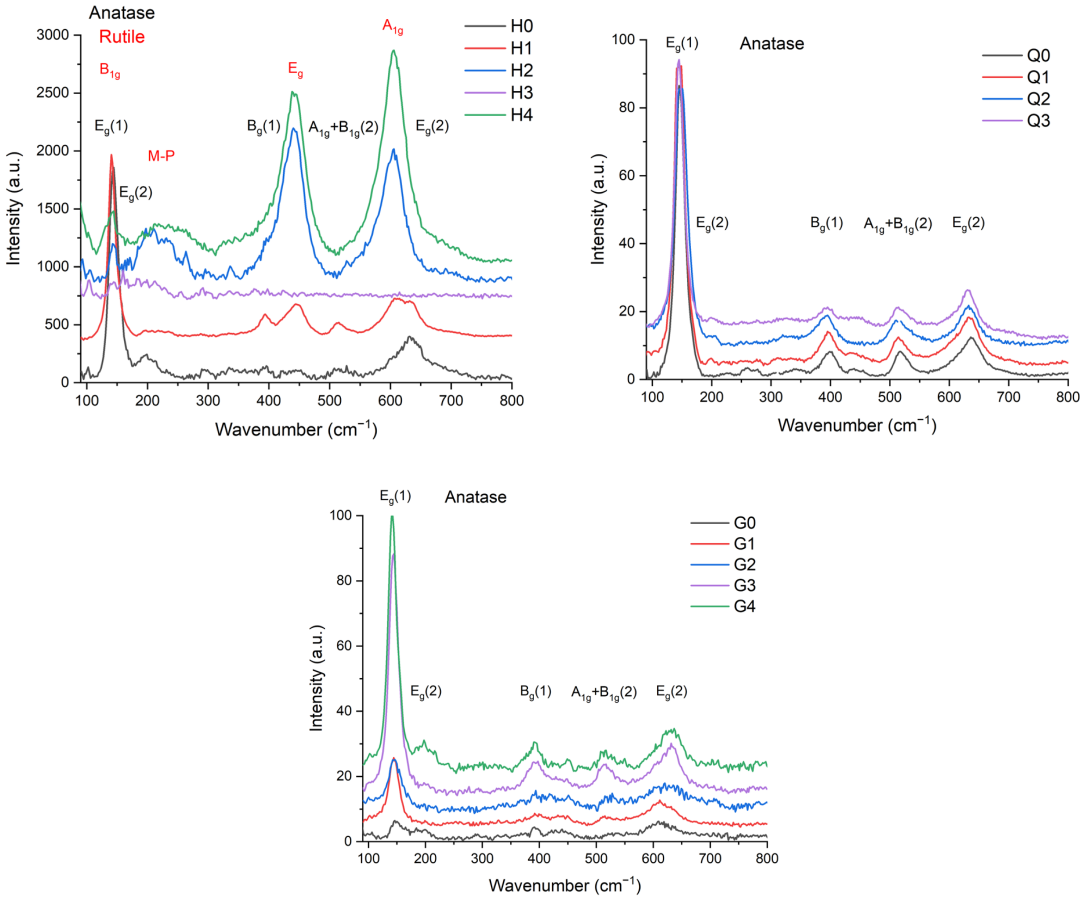

Figure 2. Raman investigation, clear TiO_2 anatase phase and carbon material, high-intensity modes at 144 and low-intensity modes at 394, 518, and 634 cm^{-1}.

Table 2. Raman mode position of samples.

Sample	Anatase					Rutile			References
	$E_{g(1)}$	$E_{g(2)}$	B_{1g}	A_{1g} & B_{1g}	$E_{g(3)}$	B_{1g}	E_g	A_{1g}	
	147.0	198.0	398.0	518.0	640	143.0	447.0	612	[56]
	144.0	197.0	399.0	513, 519	639				[57,58]
	144.0	197.0	397.0	516.0	641	143.0	447.0	612	[59]
	147.0	198.0	398.0	515.0	640	144.0	448.0	612	[60]
	143.0	196.0	394.0	512.0	630				[61]
H0	144.4	199.3	395.7	515.1	631.3	-	-	-	This work
H1	140.5	218.2	393.8	515.1	631.3	140.5	445.5	615	This work
H2	144.4	210.7	-	-	-	144.4	441.8	606	This work
H3	144.4	-	-	-	-	144.4	-	-	This work
H4	144.4	220.1	-	-	-	144.4	441.8	606	This work
G0	148.2	199.3	392.0	527.9	609.6				This work
G1	144.4	199.3	392.0	515.1	611.4				This work
G2	146.3	199.3	393.8	527.9	620.4				This work
G3	144.4	197.4	393.8	515.1	631.3				This work
G4	142.5	197.4	392.0	517.0	631.3				This work
Q0	145.2	199.2	398.9	514.7	636.3				This work
Q1	145.2	199.2	395.1	514.7	632.6				This work
Q2	147.1	199.2	395.1	516.5	632.6				This work
Q3	145.2	199.2	395.1	512.8	630.8				This work
Q4	145.2	199.2	395.1	512.8	630.7				This work

As seen in Figure 3, XRD shows the presence of TiO_2 in the anatase phase as seen by the peaks corresponding to (101), (200), (105), (107), (215), (301), (224) in samples G and Q. The same peaks at various intensities are visible for other samples and at various added CNP concentrations. The estimation of crystallite size for G samples is roughly the same size, similar to Q, where A (101) crystallites are the same size with an increase of added material.

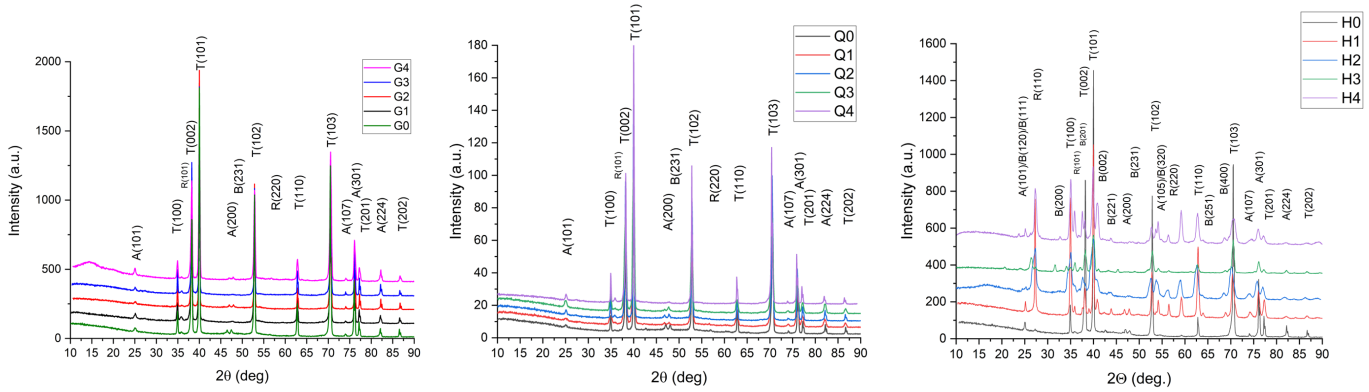

Figure 3. Influence of CNP additives on sample crystalline structure investigated with XRD for the G, Q, H series of samples.

Optical and Electrochemical Properties

Introducing carbon materials into TiO_2 shifts the optical absorption edge to the visible spectrum from 3.2 eV of anatase or 3.0 eV of rutile up to 2.7 eV, as seen in Table 3 and in Figure 4a. In the Q series, there is a slight shift of absorption edge to higher wavelengths, as seen in Figure 4a, while, on the other hand, G and H showed a large decrease of E_{gap}. Spectrophotometric data show that composite layers experience a shift of E_{gap}, depending on the amount added—from 3.21 eV to 3.06, 2.60, and 2.98 eV, respectively, in the case of Q. In comparison, synthesized nanoparticles of the H samples provide a larger shift in the E_{gap} value. A comparison of the light-induced charge carrier separation as a photocurrent response to light chopping (PCR) can be seen in Figure 4b.

Table 3. Summary of measured values and parameters.

Additive	Sample	OCP, mV	PCR, μA/cm^2	E_{gap}, eV	E_{Fb}, mV	N_D, cm^{-3}•10^{17}	k, h^{-1}
Q	Q0	−29.1 ± 0.5	2.1 ± 0.1	3.21 ± 0.02	−908.0 ± 5.0	15.4	−0.00323
	Q1	−58.7	1.4	3.06	−1004.6	17.8	−0.00505
	Q2	−26.3	1.5	3.06	−1034.0	18.2	−0.00549
	Q3	−126.1	1.8	2.61	−1015.0	28.2	−0.00434
	Q4	−156.1	2.9	2.98	−1036.0	27.8	−0.00299
G	G0	−46.5	1.5	3.13	−942.5	97.8	−0.01541
	G1	−33.8	1.4	3.05	−1011.1	21.5	−0.01512
	G2	−22.6	0.5	3.06	−959.2	3.95	−0.00746
	G3	−53.2	0.7	3.11	−947.9	4.99	−0.00192
	G4	−18.7	0.6	3.14	−704.2	68.5	−0.01021
H	H0	−109.9	1.7	3.08	−725.0	9.17	−0.0085
	H1	−238.2	11.2	2.95	−988.5	1.97	−0.01212
	H2	−256.8	12.6	2.59	−1059.8	30.1	−0.00966
	H3	−19.5	7.1	2.83	−1080.9	126.0	−0.00959
	H4	−108.7	15.3	2.84	−1060.0	133.0	−0.01269

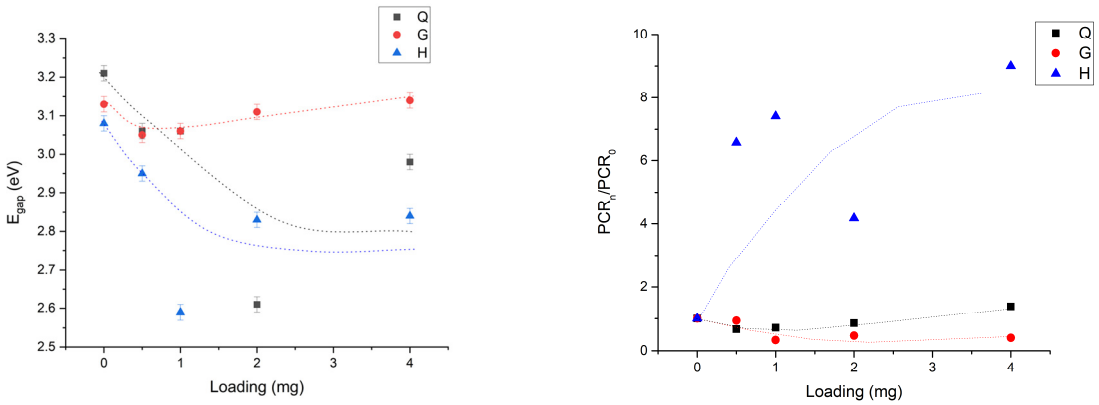

(**a**) (**b**)

Figure 4. (**a**) Influence of nanocarbon additives on TiO_2 optical absorption edge (relative change calculated as the ratio of value with added materials vs. as anodized sample). (**b**) Comparison of the light-induced PCR (right) value changes in series G (•), H (▲) and Q (■).

The addition of H and Q increases OCP and PCR values compared with pristine TiO_2, where PCR change is shown in Figure 4b. On the other hand, G decreases both OCP and PCR values, indicating reduced electron transport and an increased recombination rate, which corresponds with the higher zeta potential values measured. The increase in carbon material lowers the amount of noise and should increase the charge separation and transfer. Additionally, E_{Fb} was determined, along with charge carrier density (N_D), in order to evaluate the proposed charge separation. The G, H, and Q samples show that an increase in the loading of CNP changes not only the N_D but also the E_{FB}, as seen in Figure 5. A moderate addition of G increases the N_D, but a further increase of additive can bring it below the pristine TiO_2 level, while E_{Fb} shifts to more positive potential. On the other hand, Q and H provide an E_{Fb} shift towards more negative values, while charge carrier density increases with both additive materials. A summary of these values can be seen in Table 3.

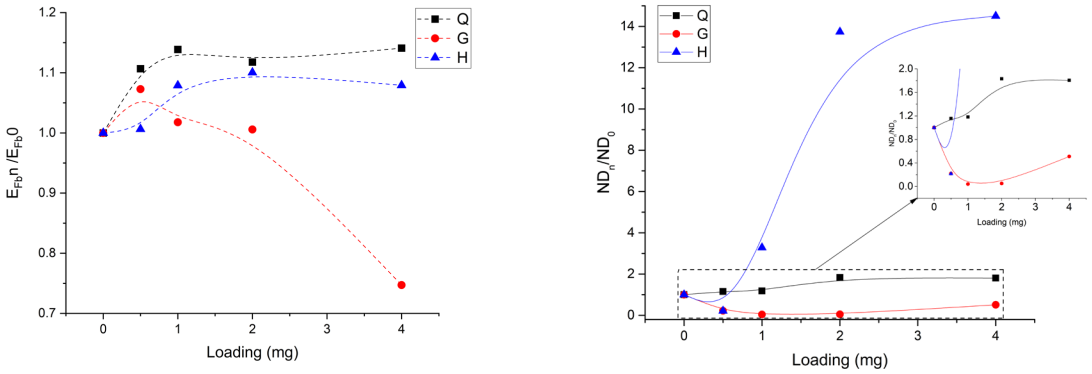

Figure 5. Flat-band potential (E_{FB}) and charge carrier density (N_D) calculated from Mott–Schottky plots for sample G (●), H (▲) and Q (■) in dependency on loading.

A well-established evaluation of photocatalytic activity is MB degradation. The decrease in solution absorbance was investigated with chosen time intervals. Concentration decrease in time, as well as calculated degradation coefficient results are depicted in Figure 6. Adding G lowers the photocatalytic activity of anodic TiO_2, which corresponds with the higher zeta potential and the lower PCR values, as shown in Table 1 and in Figures 4 and 6, respectively. Adding Q increases the activity at low added amounts, but further increasing the loading decreases the activity, as seen in Figure 6. Thus, a moderate amount of this type of carbon material is necessary for an optimal increase in photocatalytic activity. Only the addition of H increases the photocatalytic activity with an increase in the loading.

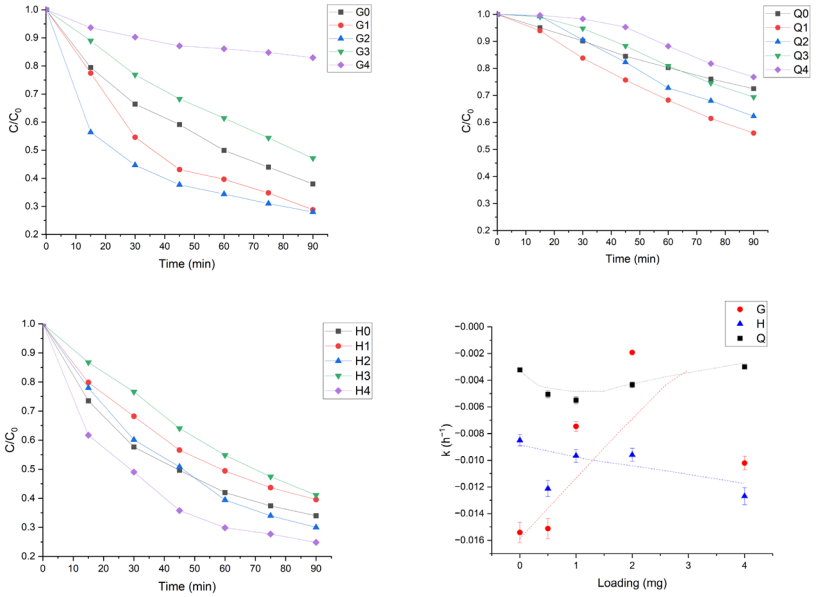

Figure 6. MB degradation graphs and dependence of the MB degradation coefficient dependence on the loading of sample H (●), Q (▲) and G (■).

4. Discussion

It was identified that, for the Q samples, there is an additional shift of TiO_2 vibration modes from 398 cm^{-1} for Q0 to 395.1 for Q1, 395.1 for Q2, and 395.1 for Q3, and that the similarity mode at 516.5 for Q0 shifted to 514.7 for Q1, 512.8 for Q2 and 514.7 for Q3. The highest mode shift can be seen from 636.3 for Q0 to 632.6 for Q1 and Q2, and 630.8 cm^{-1} for Q3; a broad low-intensity rutile mode (at 446.6 cm^{-1}) emerged from Q0. For series G the Raman vibration shift is not as visible for the mode at 144, which for G0, G1 and G2 stands at 144.4 cm^{-1}, for G3 stands at 142.5, and for G4 stands at 146.3 cm^{-1}. As the A1g&B1g vibration mode is present in all samples. The shift is more evident in the E3g

vibrational mode, where G0 is at 611.4, G1 is at 620.4, G2 is at 631.3, G3 is at 631.3 and G4 is at 609.6 cm^{-1}. This indicates that there is another phase presence in the samples, especially considering that, e.g., the rutile mode at 447 cm^{-1} is visible in these samples. Regarding carbon vibrational modes at 1350 and 1590 cm^{-1}, there are additional shifts visible in comparison with graphene quantum dot D and G vibrational modes at 1350 and 1585 cm^{-1}, respectively [62].

As for the H sample series, it is clear that only sample H0 is in pure anatase form, as seen by classic E1g, E2g, B1g, as well as A1g&B1g, but it is noteworthy that E3g has a slight shift from 640 to 631.3 cm^{-1}. Other samples show some mixture of anatase and rutile with a great increase in rutile content as seen by the appearance of B1g (144), Eg (445 and further increase of H addition shifts this vibrational mode to 441 cm^{-1}) and A1g (615 and 606 cm^{-1}).

The introduction of carbon material initiating a blue shift effect on Raman vibrational modes has been shown before [13] and single crystal heating in argon also shows blue shift of the anatase Eg(1) mode [61], which is attributed to the Ti-O vibration and, thus, to oxygen vacancy defects. Furthermore, the G and Q samples are mostly anatase with possibly small amounts of rutile for Q, as seen in XRD. The H samples are clearly transforming from anatase (at H0) to a brookite/rutile mixture (see Figure 3 H4); thus, increasing the addition of this H material promotes the phase transition. For H series we see clear changes of crystalline structure by the appearance of new peaks corresponding to the brookite phase [63,64] in addition to a strong development of a rutile peak R(110), ascribed to the thermal oxide layer by Albu et al. [65] and which should hinder photocatalytic activity. However, the brookite/rutile combination ensures larger charge carrier separation and increases catalytic activity, contrary to the study of Albu et al., in which an anatase/rutile composition was found. It is noteworthy, that in the anodic titania, thermal oxide was identified in air annealed samples rather than as a result of annealing in reducing atmospheric conditions, as in our case. It has been shown that in some cases the addition of carbon material has proven to promote the formation of rutile, as shown by Varnagiris et al. for thin films [66].

As we can see, the crystalline structure, as well as the phase composition, changes with the addition of carbon NP, but that there is a dependence on the type of carbon material as seen from clear differences in XRD and Raman data. It has been noted that carbon as a dopant can be a strong reduction agent if TiO_2 with carbon is heated in an inert atmosphere, as it was undertaken here, by defect creation such as oxygen vacancies. In combination with the inert atmosphere itself, the presence of carbon could be a promoter of phase transformation [67].

In addition, increasing the amount of CNP in the Q samples slightly lowers the amount of anatase and increases the amount of rutile, as shown by the decrease and disappearance of the A(200) peak at $2\theta = 48^\circ$ as well as the introduction of R(101) at $2\theta = 36^\circ$. Thus, the introduction of carbon materials and of graphene-based carbon nanoparticles of small size in combination with a reduced atmosphere, as per this study, promotes phase transition. In addition, and for the first time, we have shown a brookite phase in anodic TiO_2 synthesized in an inorganic electrolyte. Reducing atmosphere creates oxygen vacancies and, in combination with carbon as a reducing agent, more bonds are broken; as a result, the phase transformation can be said to be possible at lower temperatures. A proposed depiction of the process is shown in Figure 7.

As is seen in Table 3, G influences the properties of TiO_2 in a mostly negative way, which can be ascribed to the loss of electrons on G particles. As the amount of CNP increases, more electrons are trapped and lost to CNP, decreasing the overall activity due to electron recombination within G particles, which corresponds with the lower determined values of OCP, PCR, and MB degradation. On the other hand, further increase, as seen by G4, CNP seems to overtake the MB via reduction of adsorbed oxygen, which, in turn, allows the creation of •OH radicals for MB degradation. It should be noted that decreasing the flat-band potential (to more positive values) is a desirable outcome but is outweighed

by the decrease of other determined parameters. On the other hand, commercial graphene quantum dots were found to increase the photocatalytic performance of TiO_2, as can be seen by the increase in the measured parameters, including the degradation coefficient shown in Figure 6, but it is noteworthy that only small additive amounts provide a positive effect. This could be explained by increased charge separation and transfer, as well as increased light absorption as seen by the optical absorption edge that was redshifted in the Q samples, which can be attributed to changes in crystalline structure. The absorption edge redshift has been noted previously by Martins et al. [68] for titania nanoparticles. Hydrothermally treated exfoliated graphene nanoparticles have shown a positive increase in properties related to photo-catalytic activity, especially charge carrier density and MB degradation coefficient, providing much higher gains. We attribute this activity to the highest crystalline structure change and the increase of brookite phase in the samples, which is partially supported by available literature such as that describing the hydrothermal synthesis of titania nanoparticles with phase mixture [69] or the study of Kang et al. exploring anodic nanotubes in organic electrolyte and their phase transition due to annealing atmosphere [70], though we have not seen this type of phase transition empirically. Thus, the combination of structure and carbon presence allows higher charge carrier separation and light absorption. On the other hand, we have demonstrated changes in anodic titania using novel composite coating synthesis method of in situ CNP introduction.

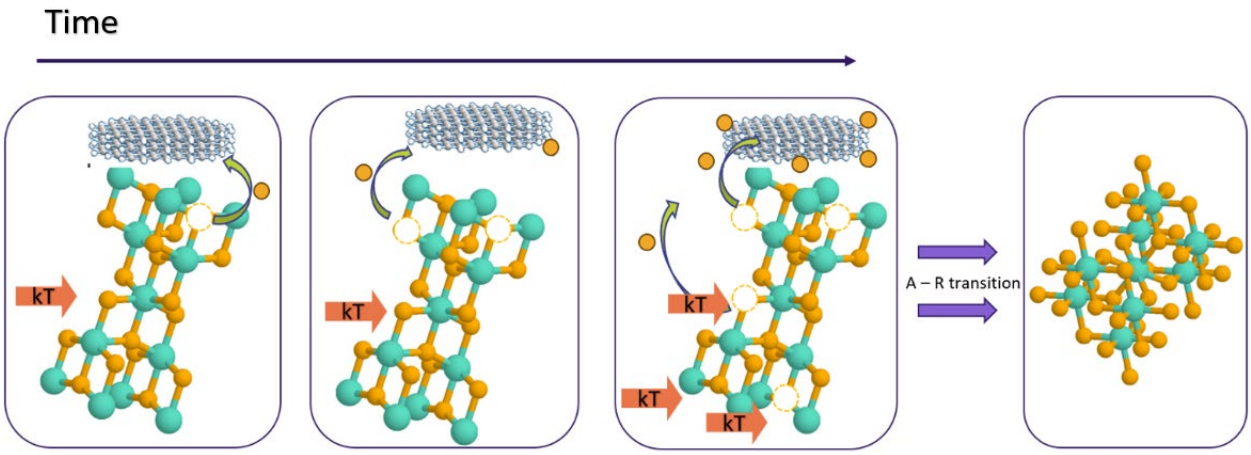

Figure 7. Phase transition model of the anatase to rutile transition in reducing atmosphere and CNP presence.

5. Conclusions

This work investigated the influence of carbon nanoparticle introduction into anodic titania for changes in photocatalytic activity. Reduced graphene sheet stacks (G) and hydrothermally treated exfoliated graphene nanoparticles (H) were compared with commercial graphene quantum dots (Q) on the basis of changes in the photoelectrochemical properties of anodic TiO_2. The addition of carbon nanoparticles was carried out with a novel composite synthesis method via the combined electrophoretic-anodic growth of TiO_2, providing an in situ additive introduction and nanotubular titania coating. The addition of carbon material changed the structural, optical, and photoelectrochemical properties of TiO_2. For the first time, the brookite phase was discovered in samples using hydrothermally treated particles, moreover, this material showed highest increase in photocatalytic activity. Introducing carbon materials in anodic TiO_2 is possible through the developed composite synthesis method and anodization growth process.

Author Contributions: Conceptualization, A.K. and J.K.; methodology, A.K. and L.G.; validation, A.K., J.K. and L.G.; formal analysis, A.K.; investigation, A.K.; data curation, J.K.; writing—original draft preparation, A.K.; writing—review and editing, L.G.; visualization, A.K.; supervision, J.K.;

project administration, A.K. and L.G.; funding acquisition, A.K. and L.G. All authors have read and agreed to the published version of the manuscript.

Funding: The research is funded by the Latvian Council of Science (project "Smart materials, photonics, technology and engineering ecosystem, project No. VPP-EM-FOTONIKA-2022/1-0001), Institute of Solid State Physics, University of Latvia, as the Center of Excellence has received funding from the European Union's Horizon 2020 Framework Programme H2020-WIDESPREAD-01-2016-2017-TeamingPhase2 under grant agreement No. 739508, project CAMART^2. Materials were funded by Scientific Research Project for Students and Young Researchers Nr. SJZ/2018/9 realized at the Institute of Solid State Physics, University of Latvia.

Institutional Review Board Statement: Not applicable.

Informed Consent Statement: Not applicable.

Data Availability Statement: The data presented in this study are available on request from the corresponding author due to ongoing research.

Acknowledgments: The author expresses gratitude to Astrida Berzina for AFM measurements.

Conflicts of Interest: The authors declare that they have no known competing financial interests or personal relationships that could have appeared to influence the work reported in this paper.

References

1. International Energy Agency. *Key World Energy Statistics*; International Energy Agency: Paris, France, 2016.
2. Mekonnen, M.M.; Gerbens-Leenes, P.W.; Hoekstra, A.Y. Future electricity: The challenge of reducing both carbon and water footprint. *Sci. Total Environ.* **2016**, *569–570*, 1282–1288. [CrossRef] [PubMed]
3. Church, J.A.; White, N.J. Sea-Level Rise from the Late 19th to the Early 21st Century. *Surv. Geophys.* **2011**, *32*, 585–602. [CrossRef]
4. Macintyre, I.G. Modern coral reefs of western Atlantic: New geological perspective. *Am. Assoc. Pet. Geol. Bull.* **2018**, *72*, 1360–1369. [CrossRef]
5. Rzymski, P.; Gwenzi, W.; Poniedziałek, B.; Mangul, S.; Fal, A. Climate warming, environmental degradation and pollution as drivers of antibiotic resistance. *Environ. Pollut.* **2024**, *346*, 123649. [CrossRef]
6. AbuQamar, S.F.; El-Saadony, M.T.; Alkafaas, S.S.; Elsalahaty, M.I.; Elkafas, S.S.; Mathew, B.T.; Aljasmi, A.N.; Alhammadi, H.S.; Salem, H.M.; Abd El-Mageed, T.A.; et al. Ecological impacts and management strategies of pesticide pollution on aquatic life and human beings. *Mar. Pollut. Bull.* **2024**, *206*, 116613. [CrossRef]
7. Mousel, D.; Palmowski, L.; Pinnekamp, J. Energy demand for elimination of organic micropollutants in municipal wastewater treatment plants. *Sci. Total Environ.* **2017**, *575*, 1139–1149. [CrossRef]
8. Gong, W.; Lewis, J.I. The politics of China's just transition and the shift away from coal. *Energy Res. Soc. Sci.* **2024**, *115*, 103643. [CrossRef]
9. Chen, D.; Ma, M.; Hu, L.; Du, Q.; Li, B.; Yang, Y.; Guo, L.; Cai, Z.; Ji, M.; Zhu, R.; et al. Characteristics of China's coal mine methane emission sources at national and provincial levels. *Environ. Res.* **2024**, *259*, 119549. [CrossRef]
10. Yang, L.; Yang, L.; Ding, L.; Deng, F.; Luo, X.B.; Luo, S.L. Principles for the Application of Nanomaterials in Environmental Pollution Control and Resource Reutilization. In *Nanomaterials for the Removal of Pollutants and Resource Reutilization*; Elsevier: Amsterdam, The Netherlands, 2018; pp. 1–23.
11. Zou, J.P.; Chen, Y.; Zhu, M.; Wang, D.; Luo, X.B.; Luo, S.L. Semiconductor-Based Nanocomposites for Photodegradation of Organic Pollutants. In *Nanomaterials for the Removal of Pollutants and Resource Reutilization*; Elsevier: Amsterdam, The Netherlands, 2018; pp. 25–58.
12. Roy, P.; Berger, S.; Schmuki, P.; Schmuki, P. TiO_2 Nanotubes: Synthesis and Applications. *Angew. Chem. Int. Ed.* **2011**, *50*, 2904–2939. [CrossRef]
13. Zhang, Z.; Tan, J.; Cheng, L.; Yang, W. Carbon nano-layer coated TiO_2 nanoparticles for efficient photocatalytic CO_2 reduction into CH_4 and CO. *Ceram. Int.* **2021**, *47*, 34106–34114. [CrossRef]
14. Chen, C.; Wen, Y.; Hu, X.; Ji, X.; Yan, M.; Mai, L.; Hu, P.; Shan, B.; Huang, Y. Na+ intercalation pseudocapacitance in graphene-coupled titanium oxide enabling ultra-fast sodium storage and long-term cycling. *Nat. Commun.* **2015**, *6*, 6929. [CrossRef] [PubMed]
15. Liu, G.; Xu, L.; Li, Y.; Guo, D.; Wu, N.; Yuan, C.; Qin, A.; Cao, A.; Liu, X. Metal-organic frameworks derived anatase/rutile heterostructures with enhanced reaction kinetics for lithium and sodium storage. *Chem. Eng. J.* **2022**, *430*, 132689. [CrossRef]
16. Yaqoob, A.A.; Ibrahim, M.N.M.; Rodríguez-Couto, S. Development and modification of materials to build cost-effective anodes for microbial fuel cells (MFCs): An overview. *Biochem. Eng. J.* **2020**, *164*, 107779. [CrossRef]
17. Qiao, Y.; Bao, S.J.; Li, C.M.; Cui, X.Q.; Lu, Z.S.; Guo, J. Nanostructured polyaniline/titanium dioxide composite anode for microbial fuel cells. *ACS Nano* **2008**, *2*, 113–119. [CrossRef]
18. Pichat, P. *Photocatalysis and Water Purification: From Fundamentals to Recent Applications*; Wiley-VCH Verlag GmbH & Co. KGaA: Weinheim, Germany, 2013.

19. Ebraheem, S.; El-Saied, A. Band Gap Determination from Diffuse Reflectance Measurements of Irradiated Lead Borate Glass System Doped with TiO_2 by Using Diffuse Reflectance Technique. *Mater. Sci. Appl.* **2013**, *4*, 324–329. [CrossRef]
20. Kmentova, H.; Kment, S.; Wang, L.; Pausova, S.; Vaclavu, T.; Kuzel, R.; Han, H.; Hubicka, Z.; Zlamal, M.; Olejnicek, J.; et al. Photoelectrochemical and structural properties of TiO_2 nanotubes and nanorods grown on FTO substrate: Comparative study between electrochemical anodization and hydrothermal method used for the nanostructures fabrication. *Catal. Today* **2016**, *287*, 130–136. [CrossRef]
21. Grimes, C.A.; Mor, G.K. *TiO_2 Nanotube Arrays*; Springer: Boston, MA, USA, 2009.
22. Zhang, J.; Zhou, P.; Liu, J.; Yu, J. New understanding of the difference of photocatalytic activity among anatase, rutile and brookite TiO_2. *Phys. Chem. Chem. Phys.* **2014**, *16*, 20382–20386. [CrossRef]
23. Wu, P.G.; Ma, C.H.; Shang, J.K. Effects of nitrogen doping on optical properties of TiO_2 thin films. *Appl. Phys. A Mater. Sci. Process.* **2005**, *81*, 1411–1417. [CrossRef]
24. Shin, S.; Kim, K.; Choi, J. Fabrication of ruthenium-doped TiO_2 electrodes by one-step anodization for electrolysis applications. *Electrochem. Commun.* **2013**, *36*, 88–91. [CrossRef]
25. Yuzer, B.; Aydın, M.I.; Con, A.H.; Inan, H.; Can, S.; Selcuk, H.; Kadmi, Y. Photocatalytic, self-cleaning and antibacterial properties of Cu(II) doped TiO_2. *J. Environ. Manag.* **2022**, *302*, 114023. [CrossRef]
26. Pan, D.; Zhang, J.; Li, Z.; Wu, M. Hydrothermal route for cutting graphene sheets into blue-luminescent graphene quantum dots. *Adv. Mater.* **2010**, *22*, 734–738. [CrossRef] [PubMed]
27. Li, K.; An, X.; Park, K.H.; Khraisheh, M.; Tang, J. A critical review of CO_2 photoconversion: Catalysts and reactors. *Catal. Today* **2014**, *224*, 3–12. [CrossRef]
28. Park, H.; Park, Y.; Kim, W.; Choi, W. Surface modification of TiO_2 photocatalyst for environmental applications. *J. Photochem. Photobiol. C Photochem. Rev.* **2013**, *15*, 1–20. [CrossRef]
29. Zeng, Z.; Chen, S.; Tan, T.T.Y.; Xiao, F.X. Graphene quantum dots (GQDs) and its derivatives for multifarious photocatalysis and photoelectrocatalysis. *Catal. Today* **2018**, *315*, 171–183. [CrossRef]
30. Jin, Z.; Owour, P.; Lei, S.; Ge, L. Graphene, graphene quantum dots and their applications in optoelectronics. *Curr. Opin. Colloid Interface Sci.* **2015**, *20*, 439–453. [CrossRef]
31. Lin, L.Y.; Nie, Y.; Kavadiya, S.; Soundappan, T.; Biswas, P. N-doped reduced graphene oxide promoted nano TiO_2 as a bifunctional adsorbent/photocatalyst for CO_2 photoreduction: Effect of N species. *Chem. Eng. J.* **2017**, *316*, 449–460. [CrossRef]
32. Gupta, S.; Smith, T.; Banaszak, A.; Boeckl, J. Graphene Quantum Dots Electrochemistry and Sensitive Electrocatalytic Glucose Sensor Development. *Nanomaterials* **2017**, *7*, 301. [CrossRef]
33. Liu, Q.; Guo, B.; Rao, Z.; Zhang, B.; Gong, J.R. Strong two-photon-induced fluorescence from photostable, biocompatible nitrogen-doped graphene quantum dots for cellular and deep-tissue imaging. *Nano Lett.* **2013**, *13*, 2436–2441. [CrossRef]
34. Silvestrov, P.G.; Efetov, K.B. Quantum dots in graphene. *Phys. Rev. Lett.* **2007**, *98*, 016802. [CrossRef]
35. Kosynkin, D.V.; Higginbotham, A.L.; Sinitskii, A.; Lomeda, J.R.; Dimiev, A.; Price, B.K.; Tour, J.M. Longitudinal unzipping of carbon nanotubes to form graphene nanoribbons. *Nature* **2009**, *458*, 872–876. [CrossRef]
36. Li, X.; Wang, X.; Zhang, L.; Lee, S.; Dai, H. Chemically derived, ultrasmooth graphene nanoribbon semiconductors. *Science* **2008**, *319*, 1229–1232. [CrossRef] [PubMed]
37. Zhao, M. Meilian Direct Synthesis of Graphene Quantum Dots with Different Fluorescence Properties by Oxidation of Graphene Oxide Using Nitric Acid. *Appl. Sci.* **2018**, *8*, 1303. [CrossRef]
38. Yang, F.; Zhao, M.; Zheng, B.; Xiao, D.; Wu, L.; Guo, Y. Influence of pH on the fluorescence properties of graphene quantum dots using ozonation pre-oxide hydrothermal synthesis. *J. Mater. Chem.* **2012**, *22*, 25471–25479. [CrossRef]
39. Pan, D.; Guo, L.; Zhang, J.; Xi, C.; Xue, Q.; Huang, H.; Li, J.; Zhang, Z.; Yu, W.; Chen, Z.; et al. Cutting sp^2 clusters in graphene sheets into colloidal graphene quantum dots with strong green fluorescence. *J. Mater. Chem.* **2012**, *22*, 3314–3318. [CrossRef]
40. Zhou, X.; Zhang, Y.; Wang, C.; Wu, X.; Yang, Y.; Zheng, B.; Wu, H.; Guo, S.; Zhang, J. Photo-Fenton reaction of graphene oxide: A new strategy to prepare graphene quantum dots for DNA cleavage. *ACS Nano* **2012**, *6*, 6592–6599. [CrossRef]
41. Zhuo, S.; Shao, M.; Lee, S.T. Upconversion and downconversion fluorescent graphene quantum dots: Ultrasonic preparation and photocatalysis. *ACS Nano* **2012**, *6*, 1059–1064. [CrossRef]
42. Pirsaheb, M.; Asadi, A.; Sillanpää, M.; Farhadian, N. Application of carbon quantum dots to increase the activity of conventional photocatalysts: A systematic review. *J. Mol. Liq.* **2018**, *271*, 857–871. [CrossRef]
43. Pan, D.; Jiao, J.; Li, Z.; Guo, Y.; Feng, C.; Liu, Y.; Wang, L.; Wu, M. Efficient separation of electron-hole pairs in graphene quantum dots by TiO_2 heterojunctions for dye degradation. *ACS Sustain. Chem. Eng.* **2015**, *3*, 2405–2413. [CrossRef]
44. Rajender, G.; Kumar, J.; Giri, P.K. Interfacial charge transfer in oxygen deficient TiO_2-graphene quantum dot hybrid and its influence on the enhanced visible light photocatalysis. *Appl. Catal. B Environ.* **2018**, *224*, 960–972. [CrossRef]
45. Wang, N.; Lin, J.; Li, Y.; Li, T.; Chen, Y.; Li, J.; Shuai, S.; Chen, L.; Chu, Z. One-pot synthesis of high performance CQDs/TiO_2 nanocomposites without carbon source addition. *J. Water Process Eng.* **2024**, *65*, 105833. [CrossRef]
46. Olins, R.; Lesnicenoks, P.; Kleperis, J.; Knoks, A.; Lukosevics, I. Electrochemical exfoliation-streamline method for synthesis of nitrogen doped graphene. *Chemija* **2021**, *32*, 9–16. [CrossRef]
47. Knoks, A.; Sika, R.; Olins, R.; Lesnicenoks, P. Investigation of carbon nanomaterial inlfuence on photocatalytic properties of TIO_2. In *Engineering for Rural Development. Proceedings of the International Scientific Conference, Jelgava, Latvia, 26–28 May 2021*; Latvia University of Life Sciences and Technologies: Jelgava, Latvia, 2021; Volume 20, pp. 1804–1813. [CrossRef]

48. Mott, N.F. The theory of crystal rectifiers. *Proc. R. Soc. Lond. A Math. Phys. Eng. Sci.* **1939**, *171*, 27–38. [CrossRef]
49. Schottky, W. Zur Halbleitertheorie der Sperrschicht- und Spitzengleichrichter. *Z. Phys.* **1939**, *113*, 367–414. [CrossRef]
50. O'Hayre, R.; Nanu, M.; Schoonman, J.; Goossens, A. Mott—Schottky and charge-transport analysis of nanoporous titanium dioxide films in air. *J. Phys. Chem. C* **2007**, *111*, 4809–4814. [CrossRef]
51. Radecka, M.; Rekas, M.; Trenczek-Zajac, A.; Zakrzewska, K. Importance of the band gap energy and flat band potential for application of modified TiO_2 photoanodes in water photolysis. *J. Power Sources* **2008**, *181*, 46–55. [CrossRef]
52. Kubelka, P. New Contributions to the Optics of Intensely Light-Scattering Materials Part II: Nonhomogeneous Layers. *J. Opt. Soc. Am.* **1954**, *44*, 330. [CrossRef]
53. Kubelka, P. New Contributions to the Optics of Intensely Light-Scattering Materials Part I. *J. Opt. Soc. Am.* **1948**, *38*, 448. [CrossRef]
54. Ubaidullah, M.; Mehmood, M.; Tanvir, M.T.; Ghani, T.; Mahmood, A.; Shah, A.; Khan, Y. Preparation of composite-layered structure of TiO_2 nanoparticles/TiO2 nanotubes and its role in dye sensitized solar cell. *J. Porous Mater.* **2021**, *28*, 555–566. [CrossRef]
55. Sreekantan, S.; Saharudin, K.A.; Lockman, Z.; Tzu, T.W. Fast-rate formation of TiO_2 nanotube arrays in an organic bath and their applications in photocatalysis. *Nanotechnology* **2010**, *21*, 365603. [CrossRef]
56. Wang, X.; Zhang, S.; Sun, L. A Two-step anodization to grow high-aspect-ratio TiO_2 nanotubes. *Thin Solid Films* **2011**, *519*, 4694–4698. [CrossRef]
57. Ohsaka, T.; Izumi, F.; Fujiki, Y. Raman spectrum of anatase, TiO_2. *J. Raman Spectrosc.* **1978**, *7*, 321–324. [CrossRef]
58. Ohsaka, T. Temperature Dependence of the Raman Spectrum in Anatase TiO_2. *J. Phys. Soc. Japan* **1980**, *48*, 1661–1668. [CrossRef]
59. Arsov, L.D.; Kormann, C.; Plieth, W. Electrochemical synthesis and in situ Raman spectroscopy of thin films of titanium dioxide. *J. Raman Spectrosc.* **1991**, *22*, 573–575. [CrossRef]
60. Balachandran, U.; Eror, N.G. Raman spectra of titanium dioxide. *J. Solid State Chem.* **1982**, *42*, 276–282. [CrossRef]
61. Akshay, V.R.; Arun, B.; Mukesh, M.; Chanda, A.; Vasundhara, M. Tailoring the NIR range optical absorption, band-gap narrowing and ferromagnetic response in defect modulated TiO_2 nanocrystals by varying the annealing conditions. *Vacuum* **2021**, *184*, 109955. [CrossRef]
62. Malard, L.M.; Pimenta, M.A.; Dresselhaus, G.; Dresselhaus, M.S. Raman spectroscopy in graphene. *Phys. Rep.* **2009**, *473*, 51–87. [CrossRef]
63. Kandiel, T.A.; Robben, L.; Alkaim, A.; Bahnemann, D. Brookite versus anatase TiO_2 photocatalysts: Phase transformations and photocatalytic activities. *Photochem. Photobiol. Sci.* **2013**, *12*, 602–609. [CrossRef]
64. López-Muñoz, M.J.; Revilla, A.; Alcalde, G. Brookite TiO_2-based materials: Synthesis and photocatalytic performance in oxidation of methyl orange and As(III) in aqueous suspensions. *Catal. Today* **2015**, *240*, 138–145. [CrossRef]
65. Albu, S.P.; Tsuchiya, H.; Fujimoto, S.; Schmuki, P. TiO_2 nanotubes—Annealing effects on detailed morphology and structure. *Eur. J. Inorg. Chem.* **2010**, *2010*, 4351–4356. [CrossRef]
66. Varnagiris, S.; Medvids, A.; Lelis, M.; Milcius, D.; Antuzevics, A. Black carbon-doped TiO_2 films: Synthesis, characterization and photocatalysis. *J. Photochem. Photobiol. A Chem.* **2019**, *382*, 111941. [CrossRef]
67. Hanaor, D.A.H.; Sorrell, C.C. Review of the anatase to rutile phase transformation. *J. Mater. Sci.* **2011**, *46*, 855–874. [CrossRef]
68. Martins, N.C.T.; Ângelo, J.; Girão, A.V.; Trindade, T.; Andrade, L.; Mendes, A. N-doped carbon quantum dots/TiO_2 composite with improved photocatalytic activity. *Appl. Catal. B Environ.* **2016**, *193*, 67–74. [CrossRef]
69. Neetu; Singh, S.; Srivastava, P.; Bahadur, L. Hydrothermal synthesized Nd-doped TiO_2 with Anatase and Brookite phases as highly improved photoanode for dye-sensitized solar cell. *Sol. Energy* **2020**, *208*, 173–181. [CrossRef]
70. Kang, X.; Chen, S. Photocatalytic reduction of methylene blue by TiO2 nanotube arrays: Effects of TiO_2 crystalline phase. *J. Mater. Sci.* **2010**, *45*, 2696–2702. [CrossRef]